

1
2
3
4
5
6
7
8
9
10
11
12
13
14
15
16
17
18
19
20
21
22
23
24
25
26
27

Articles
Discoveries section

Title

Identification of a divergent basal body assembly protein involved in land plant spermatogenesis

Shizuka Koshimizu^{1,†}, Naoki Minamino^{2,†}, Tomoaki Nishiyama³, Emiko Yoro⁴, Kazuo Ebine^{2,5}, Keiko Sakakibara⁴, Takashi Ueda^{2,5,*}, and Kentaro Yano^{1,*}

[†] These authors contributed equally

* Corresponding authors

¹ School of Agriculture, Meiji University, Kawasaki 214-8571, Japan

² Division of Cellular Dynamics, National Institute for Basic Biology, Okazaki 444-8585, Japan

³ Research Center for Experimental Modeling of Human Disease, Kanazawa University, Kanazawa 920-0934, Japan

⁴ Department of Life Science, Rikkyo University, Tokyo 171-8501, Japan

⁵ Department of Basic Biology, SOKENDAI (The Graduate University for Advanced Studies), Okazaki 444-8585, Japan

E-mail addresses of corresponding authors

Kentaro Yano : kyano@meiji.ac.jp

Takashi Ueda : tueda@nibb.ac.jp

28 **Abstract**

29 Oogamy is a form of sexual reproduction and evolved independently in animals, fungi, and plants. In
30 streptophyte plants, Charophyceae, Coleochaetophyceae, bryophytes, lycophytes, ferns
31 (monilophytes), and some gymnosperms (Cycads and Ginkgo) utilize spermatozooids as the male
32 gamete. Plant spermatozooids commonly possess characteristic structures such as the spline, which
33 consists of a microtubule array, the multilayered structure (MLS) in which the uppermost layer is
34 continuum of the spline, and multiple flagella. However, the molecular mechanisms underpinning
35 plant spermatogenesis remain to be elucidated. To identify the genes involved in plant
36 spermatogenesis, we performed computational analyses and successfully found deeply divergent
37 BLD10s by combining multiple methods and omics-data. We then validated the functions of candidate
38 genes in the liverwort *Marchantia polymorpha* and the moss *Physcomitrium patens* and found that
39 MpBLD10 and PpBLD10 are required for normal basal body and flagella formation. *Mpblid10*
40 mutants exhibited defects in remodeling of the cytoplasm and nucleus during spermatozoid formation,
41 thus MpBLD10 should be involved in chromatin reorganization and elimination of the cytoplasm
42 during spermiogenesis. Streptophyte BLD10s are orthologous to BLD10/CEP135 family proteins,
43 which function in basal body assembly, but we found that BLD10s evolved especially fast in land
44 plants and MpBLD10 might obtain additional functions in spermatozoid formation through the fast
45 molecular evolution. This study provides a successful example of combinatorial study from
46 evolutionary and molecular genetic perspectives that elucidated a function of the key protein of the
47 basal body formation that fast evolved in land plants.

48

49 **Introduction**

50 Oogamy is a form of sexual reproduction using female and male gametes. The female gamete (egg
51 cell) is non-motile and larger than the male gamete, whereas male gametes (sperm) are motile and
52 smaller than female gametes. Oogamy evolved independently in animals, fungi, and plants (Spratt
53 1971; Simpson 2018), and it is a big question what genes drove evolution to oogamy, i.e., sperm
54 production.

55 In streptophyte plants, sexual reproduction in Charophyceae, Coleochaetophyceae, and land
56 plants are via oogamy. Among these organisms, Charophyceae, Coleochaetophyceae, bryophytes,
57 lycophytes, ferns (monilophytes), and some gymnosperms (cycads and ginkgo) utilize spermatozooids
58 as the male gamete. Oogamy in streptophyte plants is presumed to have originated from a single
59 ancestor, and flagella of spermatozooids were lost independently in angiosperms, gymnosperms (in the
60 common ancestor of cupressophytes, gnetophytes and Pinaceae), and Zygnematophyceae (Hodges et
61 al. 2012). Plant spermatozooids commonly possess characteristic structures such as the spline, which
62 consists of a microtubule array, the multilayered structure (MLS) in which the uppermost layer is a
63 continuum of the spline and basal bodies are located on it, and multiple flagella. For decades, these
64 structural features of spermatozooids have been investigated mainly by transmission electron

65 microscopy (Norstog 1967; Carothers and Kreitner 1968; Kreitner and Carothers 1976; Graham and
66 McBride 1979; Carothers and Duckett 1980; Renzaglia et al. 1985; Renzaglia and Duckett 1987). As
67 reviewed by Renzaglia and Garbary (2001), in the spermatozooids of Charophyceae, bryophytes, and
68 ferns, after the MLS develops, the nucleus becomes compacted and helically elongated along the
69 spline, during which a major part of the cytoplasm is eliminated. Unlike in these species, in
70 gymnosperms, the nucleus is neither condensed nor elongated, and the cytoplasm is not eliminated.
71 The number of flagella in a spermatozoid of bryophytes or lycophytes is two, but a spermatozoid of
72 ferns forms 20 - 50 or more flagella. Gymnosperms spermatozooids possess 1,000 - 50,000 flagella.
73 Although morphological studies have been well conducted, the molecular and genetic players in plant
74 spermatogenesis remain to be identified.

75 Currently, in addition to angiosperms, the genome sequences of a variety of streptophytes
76 have been determined by progress of sequencing technologies (Rensing et al. 2008; Banks et al. 2011;
77 Bowman et al. 2017; Li et al. 2018; Nishiyama et al. 2018; Zhao et al. 2019; Li et al. 2020; Wang et al.
78 2020), and a vast amount of omics data such as transcriptome have been accumulating in an online
79 database, the Sequence Read Archive (SRA; Leinonen et al. 2010). Banks et al. (2011) reported that,
80 after gene clustering, 32 of 137 ‘angiospermLoss’ groups (defined as present in at least two of the
81 following: *Chlamydomonas* [*Chlamydomonas reinhardtii*], *Physcomitrella* [*Physcomitrium patens*],
82 and *Selaginella* [*Selaginella moellendorffii*] but not in 15 angiosperms) harbored genes exhibiting
83 similarity to flagella or basal body-related genes, consistent with the presence of flagellated cells in
84 the three organisms. We envisioned that combining the phylogenetic distribution and expression data
85 would yield a more specific set that could test their function using molecular genetic methods. We
86 selected candidate genes specifically expressed in male reproductive tissues of *Marchantia*
87 (*Marchantia polymorpha*) and *Physcomitrella* but excluded genes apparently present in
88 *Chlamydomonas* to obtain a set that is worth investigating for the function in plant spermatogenesis.
89 The functions of the candidate genes were examined in the liverwort *Marchantia polymorpha* and the
90 moss *Physcomitrium* [*Physcomitrella*] *patens* (Rensing et al. 2020), for which molecular genetic
91 techniques have been established (Schaefer 1997; Nishiyama et al. 2000; Ishizaki et al. 2008; Kubota
92 et al. 2013). Loss-of-function mutants of the candidates MpBLD10 and PpBLD10 exhibited defects in
93 basal body and flagella formation during spermatogenesis, suggesting that these genes are required for
94 normal basal body and flagella formation. BLD10s were found to be putative orthologs of BLD10 in
95 *Chlamydomonas reinhardtii* (CrBLD10), the product is required for assembly of the basal body.
96 However, BLD10s evolved fast in the land plant lineage, and loss-of-function mutations in MpBLD10
97 and PpBLD10 resulted in different phenotypes in the liverwort and moss, which were also distinct
98 from the phenotype in the chlorophyte *CrblD10* mutant. Defects in reorganizing the cytoplasm and
99 nucleus during spermatozoid formation in MpblD10 mutants suggested that MpBLD10 plays a role in
100 spermatozoid formation, in addition to the basal body formation. Thus, we present the results of a
101 successful combinatorial study encompassing phylogenetic distribution, gene expression, and

102 molecular genetics approaches, which unraveled that the function of the key component of the basal
103 body formation is diverged during plant evolution.

104

105 **Results**

106 **Four protein family groups were selected as candidates involved in spermatogenesis**

107 To identify genes involved in plant spermatogenesis, we performed *in silico* analyses combining
108 different methods as the first screening. The computational approach included the following steps
109 (supplementary fig. S1).

110 Step 1, selection of protein family groups specific to plant species that produce
111 spermatozooids. Because plant spermatozooids have structures distinct from animal sperm, such as a
112 MLS contiguous with the spline, a spiral-shaped nucleus elongated along the spline, and multiple
113 flagella, we hypothesized that the plant species producing spermatozooids would harbor specific genes
114 not present in animals that are needed to form these distinctive structures. Therefore, we classified
115 proteins of plants producing spermatozooids and animals into family groups using the OrthoFinder tool
116 (Emms and Kelly 2019) and then selected protein family groups present only in the plants producing
117 spermatozooids. In this step, we also used protein data for *Chlamydomonas*, a flagellate green alga that
118 does not produce spermatozooids, so that we could remove known flagella proteins and unrelated
119 proteins for spermatogenesis from among the candidates by exclusion of protein families contained in
120 *Chlamydomonas*. Then, 938 protein family groups remained as primary candidates (supplementary fig.
121 S1, Step 1).

122 Step 2, extraction of protein family groups composed by genes highly expressed during
123 spermatogenesis. We expected that genes involved in spermatogenesis should be highly expressed
124 during spermatogenesis. Based on RNA-seq data for tissues in the vegetative and male reproductive
125 stages in *Marchantia* (Higo et al. 2016) and *Physcomitrella* (Koshimizu et al. 2018), we extracted
126 genes exhibiting higher expression levels during male reproductive stages compared to vegetative
127 stages. For families consisting of multiple genes, we selected as candidates those in which all
128 members are highly expressed at the male reproductive stages as candidates. In this step, 165 groups
129 were retained (supplementary fig. S1, Step 2).

130 Step 3, selection of protein family groups for which member proteins exhibit low BLAST
131 similarities with animal and *Chlamydomonas* proteins. In Step 1, we excluded protein family groups
132 shared between plants and animals or *Chlamydomonas*. In this step, we further eliminated protein
133 family groups that include proteins highly similar to those of animals or *Chlamydomonas*. *Marchantia*
134 proteins in the 165 protein family groups selected in Step 2 were used for the query, and we examined
135 sequence similarities against animals and *Chlamydomonas* proteins by BLASTP searching (Altschul
136 et al. 1997; Camacho et al. 2009). For exhaustive analysis, we used 'animals' and '*Chlamydomonas*
137 *reinhardtii*' taxa of NCBI (NCBI Resource Coordinators 2018) nr datasets for the BLASTP search.
138 When high sequence similarity to an animal or *Chlamydomonas* protein was detected (e-value < 0.001

139 or coverage > 10%), we excluded the protein family group. After this step, 31 groups remained
140 (supplementary fig. S1, Step 3; and supplementary table S1).

141 Step 4, human check of the expression level data obtained in Step 2. From the *Marchantia*
142 and *Physcomitrella* expression data used in Step 2, we selected seven genes exhibiting lower
143 expression levels in the vegetative growth stage and substantial differences in expression levels
144 between the vegetative and male reproductive stages. We then selected as candidates four protein
145 family groups (Group-75, Group-89, Group-230, and Group-339) composed of seven proteins. It
146 should be noted that although we could have initially selected genes exhibiting above-mentioned
147 expression patterns, we preferred to use a strategy that narrows down the number of candidates after
148 studying the functions of a broad range of proteins that could be involved in spermatogenesis
149 (supplementary fig. S1, Step 4).

150

151 **Two protein family groups were selected as final candidates for functional analysis**

152 Regarding Group-339, the function of a highly similar protein in *Arabidopsis*, AUG7 (AT5G17620.1),
153 in delocalization of γ -tubulin in the mitotic spindle and phragmoplast was reported (Hotta et al. 2012).
154 In spermatogenesis of bryophytes, centrioles serve as the microtubule organizing centers in the
155 spindle for the final mitosis (Vaughn and Renzaglia 1998), in which γ -tubulin localizes to the
156 centriolar centrosomes (Shimamura et al. 2004). These observations suggested that the proteins of
157 Group-339 should play a role in γ -tubulin localization during spermatogenesis; thus, we reserved
158 further functional analysis for Group-339. Group-75 included four proteins each of *Marchantia* and
159 *Physcomitrella*. Because the deletion of all genes for four members would be technically difficult
160 even in *Marchantia* or *Physcomitrella*, we also reserved this group for future analysis. The
161 *Arabidopsis* protein highly similar to Group-89 is DUO3 (AT1G64570.1), which regulates male
162 germline development, and is essential for sperm cell specification and fertilization (Brownfield et al.
163 2009). It would be interesting to investigate the function of this protein in spermatogenesis in
164 bryophytes. Group-230 proteins exhibited no similarity to *Arabidopsis* proteins, but it did exhibit a
165 weak similarity to *Chlamydomonas* BLD10 (Cre10.g418250.t1.2, CrBLD10), a cartwheel protein
166 essential for assembly of the basal body that functions as the origin of flagella (Matsuura et al. 2004;
167 Hiraki et al. 2007). In Phytozome ver. 5, which the analysis by Banks et al. (2011) was based on, the
168 member of Group-230, *Selaginella* SELMODRAFT_427424 and PHYPADRAFT_69693 (v1.1, older
169 model; same locus as Pp3c9_9040V3.2, but not the same exon-intron structure prediction), were
170 placed in the same group with CrBLD10. However, the similarity was so subtle that the relation was
171 not detected in Step 3. Current Phytozome ver. 12 “Gene Ancestry” for the viridiplantae places the
172 *Physcomitrella* and *Marchantia* to different groups containing only mosses and *Marchantia*,
173 respectively. No description on the encoding gene in *Marchantia* has been made, and the
174 corresponding gene is annotated as a ‘structural maintenance of chromosomes smc family member’,
175 with no publications reporting results of functional analyses in *Physcomitrella*. Thus, we decided to

176 conduct further functional analyses for Group-89 and Group-230 consisting of one member each in
177 Marchantia, particularly focusing our interest on spermatogenesis (supplementary fig. S1, Step 5).

178

179 **Mpbl $d10$ mutants are defective in spermatozoid formation**

180 To analyze the roles of these two genes, we generated knock-out lines by genome editing using the
181 CRISPR/Cas9 system (Ran et al. 2013; Sugano et al. 2018). No mutants were obtained for the
182 *Mapoly0029s0108* gene (Group-89). For the *Mapoly0001s0460* gene (Group-230), the guide-RNA
183 sequence was designed to target the first exon (fig. 1A), and two independent lines harboring
184 frameshift mutations were obtained (fig. 1A and supplementary fig. S2A). Hereinafter, we refer to
185 Group-230 family proteins as BLD10 because the phenotype and sequence analyses suggested an
186 orthologous relationship to CrBLD10. The mutants were designated Mpbl $d10$ -1 and Mpbl $d10$ -2.
187 These mutations did not markedly affect vegetative growth of the thalli (supplementary fig. S2B) and
188 formation of antheridiophores (supplementary fig. S2C-S2E). However, moving spermatozoids of the
189 mutants were rarely observed for the mutants (supplementary movie 1-3). Intriguingly, cytoplasm
190 elimination, nuclear elongation, and flagella formation were incomplete in the mutant spermatozoids
191 compared with wild-type spermatozoids (fig. 1B-1E). Immunostaining of centrin and acetylated
192 tubulin (ac-tubulin) in spermatids was performed to observe basal bodies and the axoneme in the
193 flagella (fig. 1F-1I, Higo et al. 2018). Filaments of ac-tubulin were detected in a subpopulation of
194 Mpbl $d10$ -spermatids, but spermatids with no detectable ac-tubulin were also observed. In spermatids
195 positive for the ac-tubulin signal, short or coiled filaments in the cell bodies were frequently noted (fig.
196 1G and 1H). The puncta signals of centrin exhibiting an abnormal size were sometimes observed in
197 the mutant (fig. 1I). These results suggested that MpBLD10 plays a crucial role in spermatozoid
198 formation in Marchantia.

199 To examine the effect of the mutation in MpBLD10 at an ultrastructural level, we conducted
200 a transmission electron microscopy (TEM) analysis of spermatids and spermatozoids of the
201 Mpbl $d10$ -1 mutant. The flagella of wild-type spermatids contained an axoneme comprising two
202 central microtubules and surrounding nine doublet microtubules (fig. 2A). In the Mpbl $d10$ -1 mutant,
203 however, a major population of spermatids did not harbor flagella, and the flagella formed in a
204 subpopulation of spermatids exhibited a disordered axoneme structure (fig. 2E). No structural
205 abnormalities were detected in the Mpbl $d10$ -1 mutant MLS, a structure unique to plants that is
206 attached to the anterior mitochondrion in spermatids and consists of the spline, which is the
207 uppermost stratum containing arrayed microtubules, and a lower strata with high electron densities,
208 namely, the lamellar strip (fig. 2B and 2F). We also observed wild-type basal bodies, which contain
209 nine triplet microtubules and are attached to the spline of the MLS (fig 2C and 2D). In the Mpbl $d10$ -1
210 mutant, the wild type-like basal bodies were only occasionally observed, and amorphous
211 electron-dense regions were frequently observed instead of basal bodies (fig. 2G and 2H). These
212 results strongly suggested that MpBLD10 is required for correct assembly of the basal body and

213 flagella during spermatogenesis. Furthermore, we observed that the *Mpblld10-1* spermatozooids also
214 exhibited a defect in chromatin compaction in the nucleus (fig. 2I and 2J). Thus, *MpBLD10* might
215 also be involved in chromatin organization during spermiogenesis in Marchantia.

216

217 **PpBLD10 is required for formation of basal bodies and flagella**

218 To further examine the functions of the Group-230 proteins (BLD10s) in bryophytes, we analyzed the
219 ortholog of *MpBLD10* in *Physcomitrella*, the model of moss readily amenable to gene targeting and
220 genome editing. The Group-230 in *Physcomitrella* consists of only *Pp3c9_9040V3.2* (*PpBLD10*). We
221 generated knock-out mutants of this gene using the CRISPR-Cas9 system. *Ppblld10-22*, which has an
222 11-bp deletion in the first exon, and *Ppblld10-30*, which has an approximately 10-kbp deletion
223 between exon 1 and exon 29 of the transcript XM_024529611.1, were used in further analyses
224 (supplementary fig. S3). Although these mutants did not exhibit any marked defects in protonemata,
225 gametophores, and gametangia (supplementary fig. S4), spermatozooids of these mutants were not
226 motile; no moving mutant spermatozooids were observed (supplementary movie 4-6). Spermatids
227 lacking the signal or with coiled filaments were observed in the mutants immunostained for ac-tubulin
228 (supplementary fig. S5C-S5F), indicating that the mutants are defective in flagella formation, similar
229 to Marchantia. No marked defects in elimination of the cytoplasm and nuclear elongation of the
230 mutants were observed (supplementary fig. S6A-S6C).

231 In the TEM analysis of spermatids and spermatozooids, no axoneme structure was observed
232 in most of the spermatids in *Ppblld10-30* (supplementary fig. S7A and S7C), and amorphous
233 electron-dense regions were observed instead of basal bodies (supplementary fig. S7B and S7D). With
234 regard to the MLS, no marked defects were observed in the mutant, similar to the *Mpblld10-1* mutant
235 (supplementary fig. S7B and S7D). In contrast to the *Mpblld10-1*, no defect in chromatin compaction
236 in the nucleus was observed in *Ppblld10-30* (supplementary fig. S7E and S7F). These results suggest
237 that PpBLD10 functions in basal body- and flagella assembly, but the requirement for PpBLD10 in
238 chromatin compaction and nuclear formation differs from the case in Marchantia.

239

240 **MpBLD10 and PpBLD10 localize in basal bodies during flagella formation**

241 We next examined the subcellular localization of MpBLD10. We generated a transgenic line of
242 Marchantia expressing mCitrine-fused MpBLD10 driven by its own promoter in *Mpblld10-1*.
243 Expression of mCitrine-MpBLD10 restored the defects in spermatozoid formation and motility in the
244 mutant, indicating that this chimeric protein retains the authentic function (supplementary movie 7).
245 In this transgenic line, we traced spermiogenesis according to developmental stage as previously
246 defined (Minamino et al. 2021). In stage 0 spermatids, mCitrine-MpBLD10 was observed as two
247 closely aligned rod-like structures (fig. 3A). In stage 1 spermatids, mCitrine-positive structures were
248 located at the base of the flagella (fig. 3B). In stage 2, the mCitrine-MpBLD10 signal became weak,
249 then ultimately disappeared in subsequent stages (fig. 3C-3F). To verify the nature of these structures,

250 we performed co-immunostaining with centrin and ac-tubulin. As shown in fig. 3G,
251 mCitrine-MpBLD10 was localized in close association with centrin at the proximal side of the flagella
252 (fig. 3G). These results suggest that MpBLD10 localize in the basal body during flagella formation
253 and is then degraded after flagella formation.

254 The localization of PpBLD10 in *Physcomitrella* was examined using Citrine knock-in lines
255 (supplementary fig. S3). Spermiogenesis was observed according to the developmental stages defined
256 for *Marchantia* (Minamino et al. 2021) (supplementary fig. S8A-S8E), but in *Physcomitrella*, flagella
257 formation was slower than in *Marchantia* and began when the nuclear shape was spindle-like; thus,
258 stages 0 and 1 as defined for *Marchantia* are indistinguishable in *Physcomitrella*. PpBLD10-Citrine
259 signals were observed in stage 0-1 and stage 2 but disappeared in subsequent stages, as in *Marchantia*
260 (supplementary fig. S8A-S8E). In stage 0-1, the PpBLD10-Citrine was observed as puncta
261 (supplementary fig. S8A); in stage 2, the signal was detected in a wider region of the basal part of the
262 flagella as compared with stage 0-1 (supplementary fig. S8B and S8F). The positional relationship
263 between PpBLD10-Citrine and centrin in *Physcomitrella* could not be observed because the
264 anti-centrin antibody did not immunostain *Physcomitrella* spermatids (data not shown).

265

266 **BLD10s exist in streptophytes with flagella and evolved fast in land plants**

267 CrBLD10, to which MpBLD10 and PpBLD10 exhibit weak similarity, is an ortholog of *Homo*
268 *sapiens* CEP135 (HsCEP135) (Carvalho-Santos et al. 2010), which plays a role in early basal
269 body/centriole biogenesis (Kleylein-Sohn et al. 2007). To obtain information on BLD10 proteins in
270 the streptophyte lineage and to assess their orthology to the BLD10/CEP135 family, we searched the
271 genome, transcript, and protein sequences of species ranging from streptophyte algae to angiosperms
272 (angiosperms: *Arabidopsis thaliana* and *Oryza sativa*; gnetophytes: *Gnetum montanum*; Pinaceae:
273 *Picea abies* and *Pinus taeda*; Ginkgo: *Ginkgo biloba*; monilophytes: *Salvinia cucullata* and *Azolla*
274 *filiculoides*; lycophytes: *Selaginella moellendorffii*; bryophytes: *Anthoceros punctatus*;
275 Zygnematophyceae: *Penium margaritaceum*, *Mesotaenium endlicherianum*, and *Spiroglaea*
276 *muscicola*; Coleochaetophyceae: *Coleochaete orbicularis*; Charophyceae: *Chara braunii*;
277 Klebsormidiophyceae: *Klebsormidium nitens*; Mesostigmatophyceae: *Mesostigma viride*;
278 Chlorokybophyceae: *Chlorokybus atmophyticus*). In *Arabidopsis*, *Oryza*, *Gnetum*, *Picea*, *Pinus*,
279 *Penium*, *Mesotaenium*, and *Spiroglaea*, no hit sequences were obtained. Some of the hit sequences
280 were reconstructed based on RNA-seq data and similarity to preliminary alignments. Finally, Ginkgo
281 (GbBLD10a and GbBLD10b), *Salvinia* (Sacu_v1.1_s0007.g003760), *Azolla* (AfBLD), *Selaginella*
282 (SmBLD10), *Anthoceros* (Apun_evm.model.utg000038l.487.1), *Coleochaete* (GBSL01053926.1),
283 *Chara* (CbBLD10), *Klebsormidium* (kfl00353_0080_v1.1), *Mesostigma* (MvBLD10), and
284 *Chlorokybus* (Chrsp112S01623) were subjected to the alignment and phylogenetic analyses together
285 with MpBLD10, PpBLD10, and CrBLD10 and non-plant BLD10/CEP135 family sequences from *H.*
286 *sapiens* (HsCEP135), *Drosophila melanogaster* (DmBLD10), and *Tetrahymena thermophila*

287 (TtBLD10) as outgroup sequences (fig. 4A and supplementary fig. S9). Additionally, we included the
288 additional sequences *Adiantum capillus-veneris* MBC9850943.1, *Chlamydomonas eustigma*
289 CEUSTIGMA_g448.t1, and *Bombus impatiens* XP_012244165.1 to stabilize the alignment and
290 phylogenetic tree by dividing long branches. Here, among multiple potential isoforms, ref_seq protein
291 XP_024385379.1 was used for the phylogenetic analysis because this isoform of PpBLD10 was well
292 supported by RNA-seq data and fit the alignment better.

293 In the phylogenetic analysis, the green plant, streptophyte, and land plant genes formed a
294 clade (fig. 4A). Among land plants, the setaphytes (mosses + liverworts), and euphyllophytes formed
295 a clade with low and high bootstrap supports, respectively. Outside of land plants,
296 Coleochaetophyceae, Charophyceae, Klebsormidiophyceae, and Chlorokybophyceae branched in that
297 order, with low bootstrap support. The branches of the land plants were longer than those of
298 streptophyte algae (fig. 4A). The molecular clock hypothesis was rejected between land plants and
299 streptophyte algae, with *Chlamydomonas* as out-group by Tajima's relative rate test ($p < 0.05$; Tajima
300 1993), indicating an increase in the evolutionary rate of BLD10s in the land plant lineage. Upon
301 application of a local clock model in PAML (Yang 2007) to the dataset for green plants, such that the
302 branches of land plants after divergence from Coleochaetophyceae has different rates than all other
303 branches, land plants had an approximately 2-fold higher evolutionary rate than green algae.

304

305 **Green plant BLD10s have a novel conserved domain close to the C-terminus**

306 **Functional regions were reported for CrBLD10 and HsCEP135:** a probably essential region for the
307 function of CrBLD10 (residues 850 - 1,050; Hiraki et al. 2007), and three binding regions in
308 HsCEP135 (microtubule-binding region, residues 1 - 190; CPAP-binding region, residues 50 - 460;
309 hSAS-6-binding region, residues 416 - 1,140; Lin et al. 2013). Among streptophyte BLD10s, three
310 conserved regions were identified (fig. 4B and supplementary fig. S9). Region 1 does not seem to
311 exist in Selaginella, because the N-terminal region is annotated as a separate protein in the ref_seq
312 annotation (XP_024518287.1). The N-terminus of region 1 was not detected in either Ginkgo or
313 *Adiantum*. As such, the level of conservation shown in fig. 4B and supplementary fig. S9 is low, but
314 region 1 is conserved in other streptophytes. The microtubule-binding region and the N-terminal half
315 of the CPAP-binding region correspond to region 1 in streptophytes, but a large proportion of the
316 BLD10/CEP135 family is so divergent that the conserved residues are rare (supplementary fig. S9).
317 The C-terminal half of the CPAP-binding region was found to be mostly conserved among green algae
318 including Coleochaete, but it was shortened in land plants. Region 2 includes the probably essential
319 region of CrBLD10 and overlaps with the hSAS-6-binding region. Region 2 is a long and conserved,
320 but a large deletion of 49 residues in the CrBLD10 essential region was found in MpBLD10
321 (supplementary fig. S9). A review of RNA-seq data mapped to the region confirmed that the loss in
322 MpBLD10 was not due to an annotation error skipping an exon. The 27 N-terminal residues are
323 highly conserved in green plants. In streptophytes, region 3 is a 65-residues long highly conserved

324 region close to the C-terminus (supplementary fig. S9). Although some residues aligned, the distances
325 to human, fly, and Tetrahymena were so large that the homology is obscure, and the alignment was
326 unstable to additional insect sequences. Similarity to outside of land plants cannot be detected through
327 PSI-BLAST (Altschul et al. 1997) with land plant sequences in NCBI, and no conserved domain was
328 found in the conserved domain database (CDD; Lu et al. 2020). An examination of the alignment
329 revealed that, CrBLD10 has region 3 starting with the signature (KR)XX(ED)LE and extending to
330 (LVM)(LV)X(LI)(LM)(SA)(KR)(VL)(DE)X(DE)(RK) except Q rich block, thus it was judged to be
331 homologous. Region 3 constitutes a novel conserved domain in green plants. A 3-amino acid (aa)
332 deletion and lower conservation in the N-terminus of the region was noted in Klebsormidium. The
333 intron-exon structure is fully supported by RNA-seq data.

334

335 **Discussion**

336 In this study, we established a pipeline that allows for efficient and rapid searches of protein family
337 groups involved in plant spermatogenesis through a computational analysis of large omics datasets
338 stored in publicly available online databases. Our *in silico* approach involves two primary steps: (i)
339 selection of protein families specific to streptophytes that produce spermatozoid, and (ii) selection of
340 protein families encoded by genes highly and predominantly expressed during spermatogenesis.
341 Using this pipeline, we extracted seven genes from approximately 19,000 Marchantia genes belonging
342 to four protein family groups (Group-75, Group-89, Group-230, and Group-339). Among these
343 protein families, we conducted functional analyses of Group-89 and Group-230 in Marchantia. No
344 Group-89 mutants were obtained, but we successfully generated loss-of-function mutants for
345 Group-230 (BLD10s). We then found that the BLD10s play a crucial role in spermatogenesis in
346 Marchantia and Physcomitrella, thus showing the effectiveness and accuracy of our computational
347 selection approach. This method is applicable to the identification of genes involved in a variety of
348 biological processes other than spermatogenesis using large omics datasets.

349 Most spermatozoids of the MpblD10 mutants did not have flagella. A few spermatozoids
350 possessed short or coiled filaments within the cytoplasm (fig. 1G-1I), likely corresponding to
351 incomplete flagella observed in a TEM image (fig. 2E). Similar results were observed in PpblD10
352 mutants (supplementary fig. S5C-S5F and supplementary fig. S7C). Generally, flagella are observed
353 outside the cell body in the early stages of spermatogenesis (Minamino et al. 2021), but the immature
354 flagella-like structures remained inside the cell in the MpblD10 and PpblD10 mutants. In addition to
355 this shared characteristic of Marchantia and Physcomitrella, the MpblD10 mutants also exhibited
356 defective cytoplasm elimination, chromatin compaction, and nuclear elongation (fig. 1C-1E and fig.
357 2J), which were not observed in the PpblD10 mutants (supplementary fig. S6B and S6C and
358 supplementary fig. S7F). MpBLD10 and PpBLD10 were localized at the base of forming flagella in
359 the early stages of spermiogenesis and disappeared after flagella formation was completed (fig. 3A-3F
360 and supplementary fig. S8A-S8E). This localization, together with the close association between

361 MpBLD10 and centrin at the base of the flagella (fig. 3G), suggests that MpBLD10 and PpBLD10 are
362 basal body proteins that function in basal body assembly. MpBLD10 is likely also involved in
363 chromatin reorganization during spermiogenesis. The additional effect of the *Mpblid10* mutation on
364 phenotypes shared between *Mpblid10* and *Ppblid10* suggests that MpBLD10 plays an additional role
365 during spermiogenesis and that the functions of MpBLD10 and PpBLD10 partially diverged during
366 bryophyte evolution.

367 In the phylogenetic analysis, the branching order among streptophyte algae was congruent
368 with an organism tree based on phylotranscriptomic analyses (Wickett et al. 2014; Puttick et al. 2018;
369 Leebens-Mack et al. 2019) with low bootstrap support (fig. 4A). Although the monophyly of land
370 plant genes was supported by a high bootstrap value, among land plants, the tree was congruent with
371 the phylogeny of organisms with low bootstrap supports, except for the position of the hornwort gene.
372 The placement of hornworts sister to all other land plants has been observed at a low frequency in low
373 copy number gene phylogenies of land plants (Li et al. 2020). Based on the congruence to the
374 phylogeny, these streptophyte BLD10s are putative orthologs of CrBLD10 (fig. 4A). Flagellate
375 species in streptophytes have BLD10; conversely, species without flagella (i.e., Zygnematophyceae,
376 conifers/gnetophytes, and angiosperms) lost BLD10 (fig. 5). BLD10/CEP135 family proteins function
377 in assembly of the basal body/centriole, which is involved in cell division and serves as the basis of
378 flagella/cilia in human (Kleylein-Sohn et al. 2007; Lin et al. 2013), fly (Mottier-Pavie and Megraw
379 2009; Carvalho-Santos et al. 2012), Tetrahymena (Bayless et al. 2012), and Chlamydomonas
380 (Matsuura et al. 2004; Hiraki et al. 2007). MpBLD10 and PpBLD10 also play a role in basal body
381 assembly, similar to other BLD10/CEP135 family proteins. In accordance with the differences in
382 BLD10 sequences between land plants and Chlamydomonas, the mutant phenotypes differed from the
383 mutants of other BLD10/CEP135 family proteins; basal bodies were completely lacking and flagella
384 never observed in *Crblid10*, but incomplete basal bodies and flagella were formed in the *Mpblid10* and
385 *Ppblid10* mutants. Although DmBLD10 remains after the development of sperms in fly (Mottier-Pavie
386 and Megraw 2009), MpBLD10 and PpBLD10 disappeared, suggesting that MpBLD10 and PpBLD10
387 are necessary only during flagella formation, and no longer needed after the formation of flagella. In
388 addition, *Mpblid10* mutants exhibited defects in cytoplasmic reduction and nuclear elongation during
389 spermiogenesis, and this phenotype was observed specifically in *Marchantia* but not in *Physcomitrella*.
390 Changes in the role of basal body/centriole in the life cycle or environment of fertilization (free water,
391 limited water, or pollination droplet) in land plants might have affected the evolutionary rate of
392 BLD10s in land plants through positive selection or a relaxation of purifying selection, which cannot
393 be discerned from the current data. Note that centrioles are not observed during cell division in land
394 plants (Buschmann and Zachgo 2016) (fig. 5). Despite *Klebsormidium nitens* NIES-2285 do not show
395 flagellated cells under laboratory conditions, BLD10 expression is detected in RNA-seq data,
396 implying their role in cell division rather than flagella formation. BLD10 probably played a dual role
397 in the flagella formation and cell division in the ancestral green algae and then lost the role in cell

398 division in land plants after other microtubule organization mechanisms for chromosome separation
399 during cell division were established; thus, the protein has a sperm-specific function in bryophytes,
400 lycophytes, and ferns. BLD10 gene was lost entirely in conifers/gnetophytes and angiosperms,
401 consistent with the loss of flagellated sperm cells.

402 We successfully identified genes that function in plant spermatogenesis using an *in silico*
403 analysis. Two identified proteins, MpBLD10 and PpBLD10, are basal body proteins that exhibit a
404 higher evolutionary rate despite the importance of their role in assembly of the basal body during
405 spermatogenesis. MpBLD10 possibly acquired a new role in spermatozooids formation—specifically,
406 in cytoplasm elimination and nuclear elongation—through plant evolution. Notably, the relationship
407 that streptophyte BLD10s are putative orthologs of BLD10 was not found in a simple run of
408 OrthoFinder, and identified only after a more detailed analysis. The importance of gene loss in the
409 evolution was recently documented in various fields/cases, and phylogenetic distribution of the gene
410 involved in a particular trait coincides with the distribution of the trait (Glastad et al. 2011; Zhang et al.
411 2013; Lin et al. 2017; Griesmann et al. 2018; Sharma et al. 2018; Gluck-Thaler et al. 2020). In this
412 analysis, we demonstrated that the process can be reversed; that is, a gene responsible for the trait can
413 be identified by searching for a gene whose phylogenetic distribution coincides with the trait
414 combined with the expression at the site the trait is observed. The results of this study thus highlight
415 the power of combinatorial analyses with expression and multiple independent losses of traits and
416 underlying genes during evolution.

417

418 **Materials and Methods**

419 ***In silico* screening**

420 Ortholog groups were predicted using OrthoFinder (v2.3.3, Emms and Kelly 2019) with the protein
421 sequences of the species shown in supplementary table S2. For expression level quantification in
422 *Marchantia* and *Physcomitrella*, transcripts per million (TPM) values were calculated using RSEM
423 (v1.3.1, Li et al. 2011) with Bowtie2 (v2.3.5.1, Langmead et al. 2012) for RNA-seq data listed in
424 supplementary table S3 using the reference transcriptome datasets listed in supplementary table S2.

425

426 **Sequence searching and reconstruction of gene models**

427 BLD10 proteins in the streptophytes were searched against the genome, transcript, and protein
428 sequences using BLAST (v2.10.1+, Altschul et al. 1997; Camacho et al. 2009). In the protein datasets,
429 BLASTP searching was performed using MpBLD10 against the species shown in supplementary table
430 S2. Hit protein sequences are listed in supplementary table S4. The lengths of hit sequences in *Ginkgo*
431 and *Chara* were <600 aa (full length of MpBLD10 is 1,123 aa). Because the close gene ids implied
432 close positions in the genome, genomic locations were investigated. Gb_13822 is at the 279 Mb
433 position on Chr12; Gb_03087-Gb03089, Gb_30854, and Gb_30855 are close to the 630 Mb position
434 on Chr12; Gb_39501 is close to the 277 Mb position on Chr7. Two gene models on Chr12 were

435 reconstructed based on mapping of RNAseq data (*GbBLD10a* and *GbBLD10b*), and no reads were
436 found for Gb_39501. In Chara, we constructed a presumptive transcript (*CbBLD10*) from the genome
437 and RNA-seq data (Nishiyama et al. 2018). Azolla sequence Azfi_s0013.g013382 had a deletion in
438 the C-terminal region. The missed exons were supplied based on the RNA-seq data (Li et al. 2018),
439 and a gene model (*AfBLD10*) was constructed. In Selaginella, the hit sequence
440 SELMODRAFT_427424 had three deletions and one insertion relative to most of the green plant
441 BLD10s in the initial alignment. By investigating the genomic sequence with the preliminary
442 alignment as a guide, a gene model more similar to the conserved consensus was constructed
443 (*SmBLD10*), though the RNA-seq data of sperm-producing tissue in Selaginella were insufficient.
444 Although SELMODRAFT_427424 resides on scaffold_90, another copy (allele) is present on
445 scaffold_104, but contained an assembly gap (stretch of Ns) and was not annotated. Further,
446 transcriptome shotgun assemblies (TSA) were searched using TBLASTN at NCBI (NCBI Resource
447 Coordinators 2018) with CrBLD10. Hit transcript sequences for *Mesostigma viride* and *Coleochaete*
448 *orbicularis* were obtained (supplementary table S4). *Mesostigma* had split hits of the different contigs
449 with reasonable similarity, presumably constituting the corresponding protein. The three contigs were
450 mapped to scaffold_80 between 197,517 and 234,765. Thus, a gene model encoding 1744 residues
451 (MvBLD10) was constructed for the region mostly based on RNA-seq mapping and a little guess
452 work. The *Coleochaete orbicularis* contig appeared to contain a complete coding sequence. The
453 reconstructed gene models are shown in supplementary data 1 and 2.

454

455 **Method for reconstructing gene models based on RNA-seq data or alignment similarity**

456 Ginkgo, Azolla, Selaginella, Chara, and *Mesostigma* BLD10 sequences were reconstructed according
457 to the following method. RNA-seq data were previously published or downloaded from SRA using
458 fastq-dump (supplementary table S3). The RNA-seq data were mapped to a corresponding reference
459 genome using hisat2 (v2.2.1; Kim et al. 2019). The mapped bam files were sorted according to the
460 coordinates using samtools (Danecek et al. 2021) and then indexed. The reference sequence and
461 annotations in gff files were loaded to JBrowse-1.15.4 (Buels et al. 2016) using prepare-reference and
462 flatfile-to-json, respectively. The indexed bam files were loaded using add-bam-track. After preparing
463 the data directory of JBrowse, the data were connected to Apollo-2.1.0 for manual editing. The gene
464 model or bam read alignment was chosen for the new gene models and merged or extended in the user
465 model editing pane. For the *Ginkgo biloba* reference, the bam file could not be indexed due to its large
466 reference size (>512 Mb). Thus, the reference was cut to 500 Mb, and Chr12, at >500 Mb, were
467 named as 'Chr12b' for subsequent processing. The records of bam files were screened for Chr7 at
468 <500 Mb and Chr12, and records for Chr12 >500 Mb were placed to Chr12b, and positions were
469 subtracted by 500 million. The reference genome gff was similarly edited. Thus, Chr7, Chr12 up to
470 500 Mb, and Chr12 over 500 Mb were loaded to JBrowse and apollo2.

471

472 **Phylogenetic analyses**

473 The protein sequences HsCEP135 (ENSP00000257287), DmBLD10 (FBpp0075391), and TtBLD10
474 (TTHERM_01164140) were obtained via Ensembl (Yates et al. 2020), FlyBase (Larkin et al. 2020),
475 and TGD (Stover et al. 2006), respectively. *Adiantum capillus-veneris* MBC9850943.1,
476 *Chlamydomonas eustigma* CEUSTIGMA_g448.t1, and *Bombus impatiens* XP_012244165.1 were
477 obtained from NCBI. Multiple sequence alignment was performed using MAFFT (Katoh and
478 Standley 2013) with the accurate option E-INS-i in Jalview software (v2.10.5, Waterhouse et al. 2009).
479 The conservation level was calculated based on that used in the AMAS method for multiple sequence
480 alignment analysis (Livingstone and Barton 1993) in Jalview. A phylogenetic tree was constructed
481 based on the multiple alignment with complete deletion of gap sites using the maximum-likelihood
482 method of MEGA X software (Kumar et al. 2018), with 1,000 bootstrap replicates.
483 Jones-Taylor-Thornton (JTT) matrix-based model (Jones et al. 1992) with gamma-distribution among
484 sites and subtree-pruning-regrafting - extensive (SPR level 5) were used for amino acid substitution
485 model and heuristic methods. Protein regions used in the analyses are shown in supplementary fig. S9
486 (orange boxes). Differences in branch length between land plants and green algae were compared
487 using the local clock model in PAML4 (v4.9j; Yang 2007). Branches in land plants and the branch
488 leading to land plants after divergence with Coleochaetophyceae were assigned category #1 in the
489 comparison. JTT model was used for amino acid rate. Other parameters were the same as those of the
490 'aaml.ctl' file distributed with the software.

491

492 **Plant materials**

493 Male accession of *Marchantia*, Takaragaike-1 (Tak-1), was used for observing spermatogenesis in this
494 study. Plants were grown on 1/2× Gamborg's B5 medium containing 1.4% (w/v) agar at 22°C in
495 continuous white light. Induction of sexual organ generation by far-red irradiation was performed as
496 described previously (Chiyoda et al. 2008).

497 *Physcomitrella* Gransden 'Cove-NIBB' line (Nishiyama et al. 2000) was used as the wild
498 type. *Physcomitrella* was cultured on BCDAT medium with 0.8% (w/v) agar at 25 °C under
499 continuous light conditions for protonemata (Nishiyama et al. 2000). Protonemata were transplanted
500 into sterile peat pots (Jiffy-7; Jiffy Products International AS) and cultured approximately one month
501 at 25 °C in continuous light for gametophores. To obtain gametangia and sporophytes, the peat pots
502 containing gametophores were incubated at 15 °C under short-day (8-h light and 16-h dark)
503 conditions (Sakakibara et al. 2008).

504

505 **Transformation of *Marchantia***

506 To construct vectors for genome editing, target sequences were selected using CRISPR direct
507 (<https://crispr.dbcls.jp/>) (Naito et al. 2015), and double-stranded oligonucleotides of the target
508 sequences were inserted into the pMpGE_En03 vector (Sugano et al. 2018). The resultant gRNA

509 cassettes were introduced into the pMpGE010 vector using Gateway LR Clonase II Enzyme Mix
510 (Thermo Fisher Scientific). To express Citrine under regulation of the Mp*BLD10* promoter, 5 kb of
511 the 5' flanking region of Mp*BLD10* with a SmaI site was introduced into the pENTR/D-TOPO vector
512 (Invitrogen). The chimeric sequence was introduced into pMpGWB307 (Ishizaki et al. 2015) using
513 Gateway LR Clonase II Enzyme Mix. To construct the mCitrine-Mp*BLD10* vector, a genomic
514 fragment containing the coding region, intron, and 4 kb of the 3' flanking region of Mp*BLD10* was
515 inserted into the SmaI site of the pENTR/D-TOPO vector containing *pro*Mp*BLD10* by using an
516 In-Fusion HD cloning kit (Clontech). A silent mutation was introduced into the PAM site by inverse
517 PCR. The CDS of monomeric Citrine was introduced into the SmaI site of the pENTR/D-TOPO
518 vector containing the Mp*BLD10* genomic fragment by using an In-Fusion HD cloning kit (Clontech).
519 The chimeric sequence was introduced into pMpGWB301 (Ishizaki et al. 2015) using Gateway LR
520 Clonase II Enzyme Mix. The primer sequences are listed in supplementary table S5.

521 Transformation of *Marchantia* was performed according to previously described methods
522 (Ishizaki et al. 2008; Kubota et al. 2013). Transgenic lines were selected with 10 mg l⁻¹ hygromycin B
523 and 100 mg l⁻¹ cefotaxime for pMpGE010, and 0.5 μM chlorsulfuron and 100 mg l⁻¹ cefotaxime for
524 pMpGWB301.

525

526 **Transformation of *Physcomitrella***

527 To perform CRISPR-mediated mutagenesis, we designed oligodeoxynucleotides used as single-guide
528 RNAs (sgRNAs) targeting Pp*BLD10* (supplementary fig. S3B) using CRISPRdirect
529 (<https://crispr.dbcls.jp/>; last visited April, 2021). The annealed oligodeoxynucleotides were cloned into
530 the BsaI site of pPpU6-sgRNA (LC494193) (Gu et al. 2020). To generate genome editing mutants,
531 protoplasts were co-transformed with a total of 6 μg of circular DNAs divided as follows: 2 μg of
532 pPpU6-Pp*BLD10*-sgRNA#1 or pPpU6-Pp*BLD10*-sgRNA#2, 2 μg of pAct-Cas9 (Collonnier et al.
533 2017), and 2 μg of pBHRF (Schaefer et al. 2010). After transient hygromycin-resistance selection,
534 transformants were recovered on a non-selective medium. To detect mutations, we amplified the
535 targeting region by PCR using three sets of primers (supplementary table S5) and sequenced the
536 fragments. To generate a Citrine knock-in line, the genomic sequence corresponding to intron 31-exon
537 35 and the 3' flanking region of Pp*BLD10* were cloned into pCTRN-NPTII-2 plasmid (AB697058).
538 The Citrine-fusion plasmid was amplified by PCR using the primers listed in supplementary table S5
539 and transformed into protoplasts. Transformation for the generation of both loss-of-function mutants
540 and Citrine knock-in lines were performed as previously described (Nishiyama et al. 2000). The
541 Citrine knock-in lines were screened using DNA gel blot analysis to confirm single integrations.
542 Genomic DNA (2 μg) was digested with EcoT22I, electrophoresed on 0.8% (w/v) SeaKem GTG
543 agarose (Lonza), and transferred onto a Hybond N+ nylon membrane (GE Healthcare). Probe
544 labelling, hybridization, and detection were performed using an AlkPhos direct labelling and detection
545 system with CDP-Star (GE Healthcare). A PCR-amplified fragment of the 3' untranslated region of

546 PpBLD10 was used as a DNA probe.

547

548 **Microscopy**

549 To observe *Marchantia* spermatids, antheridia were fixed for 60 min with 4% (w/v) paraformaldehyde
550 (PFA) in PME buffer (50 mM PIPES-KOH, 5 mM EGTA, and 1 mM MgSO₄ [pH 6.8]), and treated
551 for 30 min with cell wall digestion buffer (1% [w/v] cellulase, 0.25% [w/v] pectolyase Y-23, 1% [w/v]
552 BSA, 0.1% [w/v] NP-40, 1% glucose, and 1× cComplete™ EDTA-free protease inhibitor cocktail
553 [Roche Applied Science] in PME buffer). The samples were placed on a glass slide and then covered
554 with a cover slip in PBS containing 0.1% (v/v) Hoechst33342 (Dojindo). For immunostaining of
555 *Marchantia* spermatids, antheridia were fixed for 90 min with 4% (w/v) PFA in PME buffer and
556 treated for 30 min with cell wall digestion buffer. Cells were then treated with permeabilization buffer
557 (0.01% [v/v] Triton X-100 and 1% [w/v] BSA in PME buffer) for 10 min. After washing with PME
558 buffer three times, cells were placed on a MAS-coated glass slide (Matsunami) and incubated for 30
559 min at room temperature with blocking solution (1% [w/v] BSA in PBS buffer). After removal of
560 blocking solution, the cells were incubated with primary antibody in PBS buffer at 4°C overnight.
561 After washing with PBS buffer three times, the samples were incubated for 60 min at 37°C with the
562 secondary antibody and 0.1% (v/v) Hoechst33342 in PBS buffer. After washing with PBS buffer three
563 times, the slides were mounted using ProLong Diamond Antifade reagent (Thermo Fisher Scientific).
564 Samples were observed under a confocal microscope (LSM780, Carl Zeiss) with an oil immersion
565 lens (×63). For immunostaining of *Physcomitrella* spermatids, the same method was used with
566 modifications. The duration of cell wall digesting buffer treatment was changed to 40 min. Samples
567 were observed under a confocal microscope (LSM880, Carl Zeiss) with an oil immersion lens (×63).

568 For observation of *Marchantia* spermatozooids, freshly prepared spermatozooids in distilled
569 water were observed under a dark-field microscope (Olympus) equipped with an ORCA-Flash4.0 V2
570 camera (Hamamatsu Photonics). *Physcomitrella* spermatozooids were extracted by pressing the
571 antheridia between a glass slide and a cover slip with a 0.03-mm spacer (Koshimizu et al. 2018) and
572 observed under a dark-field microscope (BS-2040T, BioTools) equipped with a Michrome 5Pro
573 camera (BioTools).

574 The obtained images were processed using ImageJ (National Institutes of Health) and
575 Photoshop (Adobe Systems) software.

576

577 **Antibodies**

578 The monoclonal antibody against acetylated tubulin was purchased from Sigma-Aldrich (T7451) and
579 used at 1/10000 dilution for immunostaining. The polyclonal antibody against centrin was described
580 previously (Higo et al. 2018) and used at 1/5000 dilution for immunostaining. Alexa Fluor 488 plus
581 goat anti-mouse IgG, Alexa Fluor 594 plus goat anti-rabbit IgG, and Alexa Fluor 680 goat anti-mouse
582 IgG were purchased from Thermo Fisher Scientific and used at 1/1000 dilution for immunostaining.

583

584 **Transmission electron microscopy**

585 To observe spermatids, antheridia of *Marchantia Tak-1*, the *Mpblid10-1* mutant, *Physcomitrella* wild
586 type, and *Ppblid10-30* were collected and fixed with 2% PFA and 2% glutaraldehyde (GA) in 0.05 M
587 cacodylate buffer (pH 7.4) at 4°C overnight. The fixed samples were washed three times with 0.05 M
588 cacodylate buffer for 30 min each and then post-fixed with 2% osmium tetroxide in 0.05 M
589 cacodylate buffer at 4°C for 3 h. The samples were dehydrated in graded ethanol solutions (50% and
590 70% ethanol for 30 min each at 4°C, 90% for 30 min at room temperature, four times with 100%
591 ethanol for 30 min at room temperature, and 100% ethanol overnight at room temperature). The
592 samples were infiltrated with propylene oxide (PO) twice for 30 min each and placed into a 50:50
593 mixture of PO and resin (Quetol-651; Nisshin EM Co.) for 3 h. The samples were transferred to 100%
594 resin and polymerized at 60°C for 48 h. To observe mature *Marchantia* spermatozooids, spermatozooids
595 of *Tak-1* and the *Mpblid10-1* mutant were collected in water, centrifuged at 5000×*g* for 3 min, and
596 fixed with 2% PFA and 2% GA in 0.05M cacodylate buffer (pH 7.4) at 4°C overnight. The fixed
597 samples were washed three times with 0.05 M cacodylate buffer for 30 min each and post-fixed with
598 2% osmium tetroxide in 0.05 M cacodylate buffer at 4°C for 2 h. The samples were dehydrated in
599 graded ethanol solutions (50% and 70% ethanol for 20 min each at 4°C, 90% for 20 min at room
600 temperature, and four times with 100% ethanol for 20 min at room temperature). The samples were
601 infiltrated with PO twice for 30 min each and placed into a 70:30 mixture of PO and resin
602 (Quetol-651; Nisshin EM Co.) for 1 h, then the tube cap was opened, and PO was allowed to
603 volatilize overnight. The samples were transferred to 100% resin and polymerized at 60°C for 48 h.
604 The polymerized resins were ultra-thin-sectioned at 70 nm with a diamond knife using an
605 ultramicrotome (Ultracut UCT; Leica) and the sections were mounted on copper grids. The sections
606 were stained with 2% uranyl acetate for 15 min at room temperature, washed with distilled water, and
607 secondary-stained with lead stain solution (Sigma-Aldrich) for 3 min at room temperature. The grids
608 were observed under a transmission electron microscope (JEM-1400Plus; JEOL Ltd.) at an
609 acceleration voltage of 100 kV. Digital images (3296×2472 pixels) were acquired using a CCD
610 camera (EM-14830RUBY2; JEOL Ltd.).

611

612

613 **Acknowledgements**

614 We thank N. Kawakami (Meiji Univ.), K. Yoshimoto (Meiji Univ.), and H. Kaku (Meiji Univ.) for
615 support in environment of experiments, F. Nogué (INRA), Y. Horiuchi (NIBB), and M. Hasebe
616 (NIBB) for providing plasmids for genome editing of *Physcomitrella*. We also thank T. Kimura
617 (Hokkaido Univ.) and M. Shimamura (Hiroshima Univ.) for anti-centrin antibody and H. Mano
618 (NIBB) for lending electron microscopy instrumentation and for general advice. Computations were
619 partially performed on the NIG supercomputer at the ROIS National Institute of Genetics and the Data

620 Integration and Analysis Facility at the National Institute for Basic Biology. Electron microscopy
621 analyses were partly supported by the EM facility of the National Institute for Physiological Sciences.
622 Rooms for cultivating *Marchantia* were provided by the Model Plant Research Facility, NIBB
623 Bioresource Center. This work was supported by JSPS KAKENHI grants to K.Y. (19H04870), K.E.
624 (19H04872), T.U. (19H05675 and 21H02515), N.M. (20K15824), T.N (15H04413 and 19K22448)
625 and K.S. (18K06367).

626

627 **Author contributions**

628 S.K. and K.Y. performed the computational analyses. N.M., K.E., and T.U. conducted the functional
629 analyses in *Marchantia*. S.K., E.Y., and K.S. conducted the functional analyses in *Physcomitrella*. S.K.
630 and T.N. performed sequence and phylogenetic analyses. All authors analyzed the data and
631 participated in writing the manuscript.

632

633 **Figure legends**

634 Fig. 1. *Mpblld10* mutants exhibit severe defects in spermatozoid formation. (A) Schematic structure of
635 the *MpBLD10* (Mapoly0001s0460) gene. Nucleotide and amino acid sequences around mutation sites
636 in wild-type (WT) and *Mpblld10-1* are aligned. The target and PAM sequences are indicated by
637 underlining and bold font, respectively. (B-E) Maximum-intensity projection images of spermatozooids
638 of wild type (B), *Mpblld10-1* (C and D), and *Mpblld10-2* (E) stained with Hoechst33342. Scale bars =
639 10 μm (F-I) Maximum-intensity projection images of spermatids immunostained with anti-centrin and
640 anti-acetylated tubulin antibodies. Nuclei were visualized using Hoechst33342. Blue, green, and
641 magenta pseudo colors indicate Hoechst33342, Alexa 488, and Alexa 594, respectively. Scale bars = 5
642 μm .

643

644 Fig. 2. Transmission electron microscopy (TEM) of spermatids and spermatozooids in wild type and
645 *Mpblld10-1*. (A-H) TEM images in spermatids of wild type (A-D) and *Mpblld10-1* (E-H). Axonemes in
646 flagella (A and E), multilayered structures (B and F), and basal bodies (C, D, G, and H) are shown. (I
647 and J) TEM images of nuclei in spermatozooids of wild type (I) and *Mpblld10-1* (J). Scale bars = 200
648 nm.

649

650 Fig. 3. Subcellular localization of the MpBLD10 protein. (A-F) Differential interference contrast
651 microscopy (DIC) and maximum-intensity projection images of spermatids and spermatozooids
652 expressing mCitrine-MpBLD10 (green) driven by its own promoter at stage 0 (A), stage 1 (B), stage 2
653 (C), stage 3 (D), stage 4 (E), and stage 5 (F); nuclei were stained with Hoechst33342 (blue).
654 Developmental stages were classified according to Minamino et al. (2021). (G) Maximum-intensity
655 projection images of a spermatid expressing mCitrine-MpBLD10 (green) immunostained with
656 anti-centrin (magenta) and anti-acetylated tubulin (yellow) antibodies. The nucleus was stained with

657 Hoechst33342 (blue). Scale bars = 5 μ m.

658

659 Fig. 4. Comparisons of BLD10/CEP135 family protein sequences. (A) Phylogenetic tree of
660 BLD10/CEP135 family proteins. Out-groups are Tetrahymena, human, and insects. Salmon, yellow,
661 green, blue, purple, and gray background colors indicate gymnosperms, monilophytes, lycophytes,
662 bryophytes, streptophyte algae, and chlorophytes, respectively. Branch lengths are proportional to the
663 estimated number of amino acid substitutions/site (scale upper left). (B) Architecture of the
664 MpBLD10 sequence (gaps removed) with conservation level among BLD10 proteins in the
665 streptophytes in (A). Three conserved regions are indicated. Values of conservation levels were
666 obtained using Jalview software.

667

668 Fig. 5. Existence of BLD10 proteins, flagella (basal body), and centriole during cell division in the
669 plant species. Orange dots show presumed flagella loss. Groups indicated by gray color were not
670 investigated due to insufficient sequence data. For phylogenetic relationships and presence of
671 centrioles, refer to Puttick et al. (2018) and Buschmann and Zachgo (2016), respectively.

672

673 **References**

- 674 Altschul SF, Madden TL, Schäffer AA, Zhang J, Zhang Z, Miller W, Lipman DJ. 1997. Gapped
675 BLAST and PSI-BLAST: a new generation of protein database search programs. *Nucleic Acids Res.*
676 25:3389–3402.
- 677 Banks JA, Nishiyama T, Hasebe M, Bowman JL, Gribskov M, DePamphilis C, Albert VA, Aono N,
678 Aoyama T, Ambrose BA, et al. 2011. The Selaginella genome identifies genetic changes associated
679 with the evolution of vascular plants. *Science* 332:960–963.
- 680 Bayless BA, Giddings TH, Winey M, Pearson CG. 2012. Bld10/Cep135 stabilizes basal bodies to
681 resist cilia-generated forces. *Mol. Biol. Cell* 23:4820–4832.
- 682 Bowman JL, Kohchi T, Yamato KT, Jenkins J, Shu S, Ishizaki K, Yamaoka S, Nishihama R,
683 Nakamura Y, Berger F, et al. 2017. Insights into land plant evolution garnered from the *Marchantia*
684 *polymorpha* genome. *Cell* 171:287–304.e15.
- 685 Brownfield L, Hafidh S, Durbarry A, Khatab H, Sidorova A, Doerner P, Twell D. 2009. *Arabidopsis*
686 DUO POLLEN3 is a key regulator of male germline development and embryogenesis. *Plant Cell*
687 21:1940–1956.
- 688 Buels R, Yao E, Diesh CM, Hayes RD, Munoz-Torres M, Helt G, Goodstein DM, Elsik CG, Lewis SE,
689 Stein L, et al. 2016. JBrowse: a dynamic web platform for genome visualization and analysis. *Genome*
690 *Biol.* 17:66.
- 691 Buschmann H, Zachgo S. 2016. The evolution of cell division: from streptophyte algae to land plants.
692 *Trends Plant Sci.* 21:872–883.
- 693 Camacho C, Coulouris G, Avagyan V, Ma N, Papadopoulos J, Bealer K, Madden TL. 2009. BLAST+:

- 694 architecture and applications. *BMC Bioinformatics* 10:421.
- 695 Carothers ZB, Duckett JG. 1980. The bryophyte spermatozoid: a source of new phylogenetic
696 information. *Bull. Torrey Bot. Club* 107:281.
- 697 Carothers ZB, Kreitner GL. 1968. Studies of spermatogenesis in the Hepaticae. II. Blepharoplast
698 structure in the spermatid of *Marchantia*. *J. Cell Biol.* 36:603–616.
- 699 Carvalho-Santos Z, Machado P, Branco P, Tavares-cadete F, Rodrigues-martins A, Pereira-leal JB,
700 Bettencourt-dias M. 2010. Stepwise evolution of the centriole-assembly pathway. *J. Cell Sci.*
701 123:1414–1426.
- 702 Chiyoda S, Ishizaki K, Kataoka H, Yamato KT, Kohchi T. 2008. Direct transformation of the liverwort
703 *Marchantia polymorpha* L. by particle bombardment using immature thalli developing from spores.
704 *Plant Cell Rep.* 27:1467–1473.
- 705 Collonnier C, Guyon-Debast A, Maclot F, Mara K, Charlot F, Nogué F. 2017. Towards mastering
706 CRISPR-induced gene knock-in in plants: survey of key features and focus on the model
707 *Physcomitrella patens*. *Methods* 121–122:103–117.
- 708 Danecek P, Bonfield JK, Liddle J, Marshall J, Ohan V, Pollard MO, Whitwham A, Keane T, McCarthy
709 SA, Davies RM, et al. 2021. Twelve years of SAMtools and BCFtools. *Gigascience* 10:giab008.
- 710 Emms DM, Kelly S. 2019. OrthoFinder: phylogenetic orthology inference for comparative genomics.
711 *Genome Biol.* 20:238.
- 712 Glastad KM, Hunt BG, Yi S V., Goodisman MAD. 2011. DNA methylation in insects: on the brink of
713 the epigenomic era. *Insect Mol. Biol.* 20:553–565.
- 714 Gluck-Thaler E, Cerutti A, Perez-Quintero AL, Butchacas J, Roman-Reyna V, Madhavan VN,
715 Shantharaj D, Merfa M V., Pesce C, Jauneau A, et al. 2020. Repeated gain and loss of a single gene
716 modulates the evolution of vascular plant pathogen lifestyles. *Sci. Adv.* 6:4516–4529.
- 717 Graham LE, McBride GE. 1979. The occurrence and phylogenetic significance of a multilayered
718 structure in coleochaete spermatozooids. *Am. J. Bot.* 66:887-894.
- 719 Griesmann M, Chang Y, Liu X, Song Y, Haberer G, Crook MB, Billault-Penneteau B, Laressergues
720 D, Keller J, Imanishi L, et al. 2018. Phylogenomics reveals multiple losses of nitrogen-fixing root
721 nodule symbiosis. *Science* 361:eaat1743.
- 722 Gu N, Tamada Y, Imai A, Palfalvi G, Kabeya Y, Shigenobu S, Ishikawa M, Angelis KJ, Chen C,
723 Hasebe M. 2020. DNA damage triggers reprogramming of differentiated cells into stem cells in
724 *Physcomitrella*. *Nat. Plants* 6:1098–1105.
- 725 Higo A, Kawashima T, Borg M, Zhao M, López-vidriero I, Sakayama H, Montgomery SA, Sekimoto
726 H, Hackenberg D, Shimamura M, et al. 2018. Transcription factor DUO1 generated by
727 neo-functionalization is associated with evolution of sperm differentiation in plants. *Nat. Commun.*
728 9:1–13.
- 729 Higo A, Niwa M, Yamato KT, Yamada L, Sawada H, Sakamoto T, Kurata T, Shirakawa M, Endo M,
730 Shigenobu S, et al. 2016. Transcriptional framework of male gametogenesis in the liverwort

- 731 *Marchantia polymorpha* L. *Plant Cell Physiol.* 57:325–338.
- 732 Hiraki M, Nakazawa Y, Kamiya R. 2007. Report Bld10p constitutes the cartwheel-spoke tip and
733 stabilizes the 9-fold symmetry of the centriole. *Curr. Biol.* 17:1778–1783.
- 734 Hodges ME, Wickstead B, Gull K, Langdale JA. 2012. The evolution of land plant cilia. *New Phytol.*
735 195:526–540.
- 736 Hotta T, Kong Z, Ho CMK, Zeng CJT, Horio T, Fong S, Vuong T, Lee YRJ, Liu B. 2012.
737 Characterization of the *Arabidopsis* augmin complex uncovers its critical function in the assembly of
738 the acentrosomal spindle and phragmoplast microtubule arrays. *Plant Cell* 24:1494–1509.
- 739 Ishizaki K, Chiyoda S, Yamato KT, Kohchi T. 2008. Agrobacterium-mediated transformation of the
740 haploid liverwort *Marchantia polymorpha* L., an emerging model for plant biology. *Plant Cell Physiol.*
741 49:1084–1091.
- 742 Ishizaki K, Nishihama R, Ueda M, Inoue K, Ishida S, Nishimura Y, Shikanai T, Kohchi T. 2015.
743 Development of gateway binary vector series with four different selection markers for the liverwort
744 *Marchantia polymorpha*. *PLoS One* 10:e0138876.
- 745 Jones DT, Taylor WR, Thornton JM. 1992. The rapid generation of mutation data matrices from
746 protein sequences. *Bioinformatics* 8:275–282.
- 747 Katoh K, Standley DM. 2013. MAFFT multiple sequence alignment software version 7:
748 improvements in performance and usability. *Mol. Biol. Evol.* 30:772–780.
- 749 Kim D, Paggi JM, Park C, Bennett C, Salzberg SL. 2019. Graph-based genome alignment and
750 genotyping with HISAT2 and HISAT-genotype. *Nat. Biotechnol.* 37:907–915.
- 751 Kleylein-Sohn J, Westendorf J, Clech M Le, Habedanck R, Stierhof Y, Nigg EA. 2007. Plk4-Induced
752 centriole biogenesis in human cells. *Dev. Cell* 13:190–202.
- 753 Koshimizu S, Kofuji R, Sasaki-Sekimoto Y, Kikkawa M, Shimojima M, Ohta H, Shigenobu S,
754 Kabeya Y, Hiwatashi Y, Tamada Y, et al. 2018. *Physcomitrella* MADS-box genes regulate water
755 supply and sperm movement for fertilization. *Nat. Plants* 4:36–45.
- 756 Kreitner GL, Carothers ZB. 1976. Studies of spermatogenesis in the hepaticae V. Blepharoplast
757 development in *Marchantia polymorpha*. *Am. J. Bot.* 63:545.
- 758 Kubota A, Ishizaki K, Hosaka M, Kohchi T. 2013. Efficient Agrobacterium-mediated transformation
759 of the liverwort *Marchantia polymorpha* using regenerating thalli. *Biosci. Biotechnol. Biochem.*
760 77:167–172.
- 761 Kumar S, Stecher G, Li M, Knyaz C, Tamura K. 2018. MEGA X: molecular evolutionary genetics
762 analysis across computing platforms. *Mol. Biol. Evol.* 35:1547–1549.
- 763 Larkin A, Marygold SJ, Antonazzo G, Attrill H, dos Santos G, Garapati P V., Goodman JL, Sian
764 Gramates L, Millburn G, Strelets VB, et al. 2021. FlyBase: updates to the *Drosophila melanogaster*
765 knowledge base. *Nucleic Acids Res.* 49:D899–D907.
- 766 Leebens-Mack JH, Barker MS, Carpenter EJ, Deyholos MK, Gitzendanner MA, Graham SW, Grosse
767 I, Li Z, Melkonian M, Mirarab S, et al. 2019. One thousand plant transcriptomes and the

- 768 phylogenomics of green plants. *Nature* 574:679–685.
- 769 Leinonen R, Sugawara H, Shumway M. 2011. The Sequence Read Archive. *Nucleic Acids Res.*
770 39:D19–D21.
- 771 Li FW, Brouwer P, Carretero-Paulet L, Cheng S, De Vries J, Delaux PM, Eily A, Koppers N, Kuo LY,
772 Li Z, et al. 2018. Fern genomes elucidate land plant evolution and cyanobacterial symbioses. *Nat.*
773 *Plants* 4:460–472.
- 774 Li FW, Nishiyama T, Waller M, Frangedakis E, Keller J, Li Z, Fernandez-Pozo N, Barker MS,
775 Bennett T, Blázquez MA, et al. 2020. *Anthoceros* genomes illuminate the origin of land plants and the
776 unique biology of hornworts. *Nat. Plants* 6:259–272.
- 777 Lin JJ, Wang FY, Li WH, Wang TY. 2017. The rises and falls of opsin genes in 59 ray-finned fish
778 genomes and their implications for environmental adaptation. *Sci. Rep.* 7:1–13.
- 779 Lin YC, Chang C, Hsu W, Tang CC, Lin Yi-nan, Chou E, Wu C, Tang TK. 2013. Human
780 microcephaly protein CEP135 binds to hSAS-6 and CPAP, and is required for centriole assembly.
781 *EMBO J.* 32:1141–1154.
- 782 Livingstone CD, Barton GJ. 1993. Protein sequence alignments: a strategy for the hierarchical
783 analysis of residue conservation. *Bioinformatics* 9:745–756.
- 784 Lu S, Wang J, Chitsaz F, Derbyshire MK, Geer RC, Gonzales NR, Gwadz M, Hurwitz DI, Marchler
785 GH, Song JS, et al. 2020. CDD/SPARCLE: the conserved domain database in 2020. *Nucleic Acids*
786 *Res.* 48:D265–D268.
- 787 Matsuura K, Lefebvre PA, Kamiya R, Hirono M. 2004. Bld10p, a novel protein essential for basal
788 body assembly in *Chlamydomonas*: localization to the cartwheel, the first ninefold symmetrical
789 structure appearing during assembly. *J. Cell Biol.* 165:663–671.
- 790 Minamino N, Norizuki T, Mano S, Ebine K, Ueda T. 2021. Remodeling of organelles and
791 microtubules during spermiogenesis in the liverwort *Marchantia polymorpha*.
792 bioRxiv:2021.07.10.451882
- 793 Mottier-Pavie V, Megraw TL. 2009. *Drosophila* Bld10 is a centriolar protein that regulates centriole,
794 basal body, and motile cilium assembly. *Mol. Biol. Cell* 20:2605–2614.
- 795 Naito Y, Hino K, Bono H, Ui-Tei K. 2015. CRISPRdirect: software for designing CRISPR/Cas guide
796 RNA with reduced off-target sites. *Bioinformatics* 31:1120–1123.
- 797 NCBI Resource Coordinators. 2018. Database resources of the National Center for Biotechnology
798 Information. *Nucleic Acids Res.* 46:D8–D13.
- 799 Nishiyama T, Hiwatashi Y, Sakakibara K, Kato M, Hasebe M. 2000. Tagged mutagenesis and
800 gene-trap in the moss, *Physcomitrella patens* by shuttle mutagenesis. *DNA Res.* 7:9–18.
- 801 Nishiyama T, Sakayama H, de Vries J, Buschmann H, Saint-Marcoux D, Ullrich KK, Haas FB,
802 Vanderstraeten L, Becker D, Lang D, et al. 2018. The *Chara* genome: secondary complexity and
803 implications for plant terrestrialization. *Cell* 174:448–464.e24.
- 804 Norstog K. 1967. Fine structure of the spermatozoid of *Zamia* with special reference to the flagellar

- 805 apparatus. *Am. J. Bot.* 54:831.
- 806 Puttick MN, Morris JL, Williams TA, Cox CJ, Edwards D, Kenrick P, Pressel S, Wellman CH,
807 Schneider H, Pisani D, et al. 2018. The interrelationships of land plants and the nature of the ancestral
808 embryophyte. *Curr. Biol.* 28:733-745.e2.
- 809 Rensing SA, Goffinet B, Meyberg R, Wu SZ, Bezanilla M. 2020. The moss *Physcomitrium*
810 (*Physcomitrella*) *patens*: a model organism for non-seed plants. *Plant Cell* 32:1361–1376.
- 811 Rensing SA, Lang D, Zimmer AD, Terry A, Salamov A, Shapiro H, Nishiyama T, Perroud P-F,
812 Lindquist EA, Kamisugi Y, et al. 2008. The *Physcomitrella* genome reveals evolutionary insights into
813 the conquest of land by plants. *Science* 319:64–69.
- 814 Renzaglia KS, Carothers ZB, Duckett JG. 1985. Comparative ultrastructural studies of
815 spermatogenesis in the Metzgeriales (Hepaticae). I. The blepharoplast of *Pallavicinia lyellii*. *Am. J.*
816 *Bot.* 72:588–595.
- 817 Renzaglia KS, Duckett JG. 1987. Spermatogenesis in *Blasia pusilla*: from young antheridium
818 through mature spermatozoid. *Bryologist* 90:419–449.
- 819 Renzaglia KS, Garbary DJ. 2001. Motile gametes of land plants: diversity, development, and
820 evolution. *CRC. Crit. Rev. Plant Sci.* 20:107–213.
- 821 Sakakibara K, Nishiyama T, Deguchi H, Hasebe M. 2008. Class 1 KNOX genes are not involved in
822 shoot development in the moss *Physcomitrella patens* but do function in sporophyte development.
823 *Evol. Dev.* 10:555–566.
- 824 Schaefer DG, Delacote F, Charlot F, Vrielynck N, Guyon-Debast A, Le Guin S, Neuhaus JM,
825 Doutriaux MP, Nogué F. 2010. RAD51 loss of function abolishes gene targeting and de-represses
826 illegitimate integration in the moss *Physcomitrella patens*. *DNA Repair (Amst)*. 9:526–533.
- 827 Schaefer DG, Zrýd JP. 1997. Efficient gene targeting in the moss *Physcomitrella patens*. *Plant J.*
828 11:1195–1206.
- 829 Sharma V, Hecker N, Roscito JG, Foerster L, Langer BE, Hiller M. 2018. A genomics approach
830 reveals insights into the importance of gene losses for mammalian adaptations. *Nat. Commun.* 9:1–9.
- 831 Shimamura M, Brown RC, Lemmon BE, Akashi T, Mizuno K, Nishihara N, Tomizawa KI, Yoshimoto
832 K, Deguchi H, Hosoya H, et al. 2004. γ -tubulin in basal land plants: characterization, localization, and
833 implication in the evolution of acentriolar microtubule organizing centers. *Plant Cell* 16:45–59.
- 834 Simpson MG. 2018. Evolution and diversity of green and land plants. In: *Plant systematics* (3rd
835 edition). Amsterdam: Elsevier Science. pp. 55–74.
- 836 Spratt NT. 1971. *Developmental biology*. Belmont: Wadsworth Publishing Company
- 837 Stover NA, Krieger CJ, Binkley G, Dong Q, Fisk DG, Nash R, Sethuraman A, Weng S, Cherry JM.
838 2006. Tetrahymena Genome Database (TGD): a new genomic resource for *Tetrahymena thermophila*
839 research. *Nucleic Acids Res.* 34:D500–D503.
- 840 Sugano SS, Nishihama R, Shirakawa M, Takagi J, Matsuda Y, Ishida S, Shimada T, Hara-Nishimura I,
841 Osakabe K, Kohchi T. 2018. Efficient CRISPR/Cas9-based genome editing and its application to

- 842 conditional genetic analysis in *Marchantia polymorpha*. *PLoS One* 13:e0205117.
- 843 Tajima F. 1993. Simple methods for testing the molecular evolutionary clock hypothesis. *Genetics*
844 135:599–607.
- 845 Vaughn KC, Renzaglia KS. 1998. Origin of bicentrioles in Anthocerotale spermatogenous cells. In:
846 Bryology for the Twenty-first Century. London: Routledge. pp. 189–203.
- 847 Wang S, Li L, Li H, Sahu SK, Wang H, Xu Y, Xian W, Song B, Liang H, Cheng S, et al. 2020.
848 Genomes of early-diverging streptophyte algae shed light on plant terrestrialization. *Nat. Plants*
849 6:95–106.
- 850 Waterhouse AM, Procter JB, Martin DMA, Clamp M, Barton GJ. 2009. Jalview version 2-A multiple
851 sequence alignment editor and analysis workbench. *Bioinformatics* 25:1189–1191.
- 852 Wickett NJ, Mirarab S, Nguyen N, Warnow T, Carpenter E, Matasci N, Ayyampalayam S, Barker MS,
853 Burleigh JG, Gitzendanner MA, et al. 2014. Phylotranscriptomic analysis of the origin and early
854 diversification of land plants. *Proc. Natl. Acad. Sci. USA*. 111:E4859–E4868.
- 855 Wingfield J, Lechtreck K-F. 2018. *Chlamydomonas* basal bodies as flagella organizing centers. *Cells*
856 7:79.
- 857 Yang Z. 2007. PAML 4: Phylogenetic analysis by maximum likelihood. *Mol. Biol. Evol.*
858 24:1586–1591.
- 859 Yates AD, Achuthan P, Akanni W, Allen James, Allen Jamie, Alvarez-Jarreta J, Amode MR, Armean
860 IM, Azov AG, Bennett R, et al. 2020. Ensembl 2020. *Nucleic Acids Res.* 48:D682–D688.
- 861 Zhang R, Guo C, Zhang W, Wang P, Li L, Duan X, Du Q, Zhao L, Shan H, Hodges SA, et al. 2013.
862 Disruption of the petal identity gene APETALA3-3 is highly correlated with loss of petals within the
863 buttercup family (Ranunculaceae). *Proc. Natl. Acad. Sci. USA*. 110:5074–5079.
- 864 Zhao YP, Fan G, Yin PP, Sun S, Li N, Hong X, Hu G, Zhang H, Zhang FM, Han JD, et al. 2019.
865 Resequencing 545 ginkgo genomes across the world reveals the evolutionary history of the living
866 fossil. *Nat. Commun.* 10:1–10.
- 867

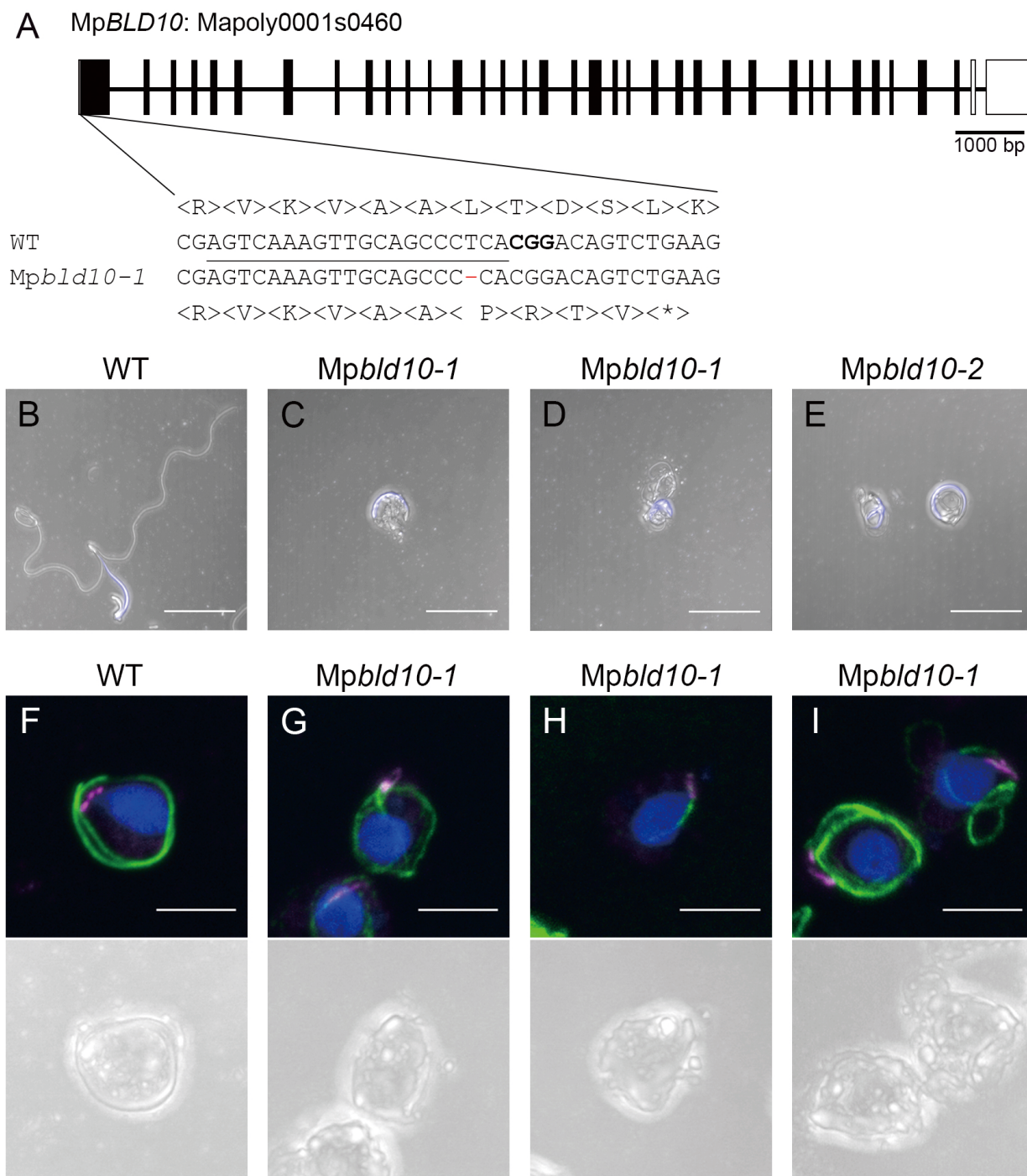


Fig. 1. *Mpblid10* mutants exhibit severe defects in spermatozoid formation.

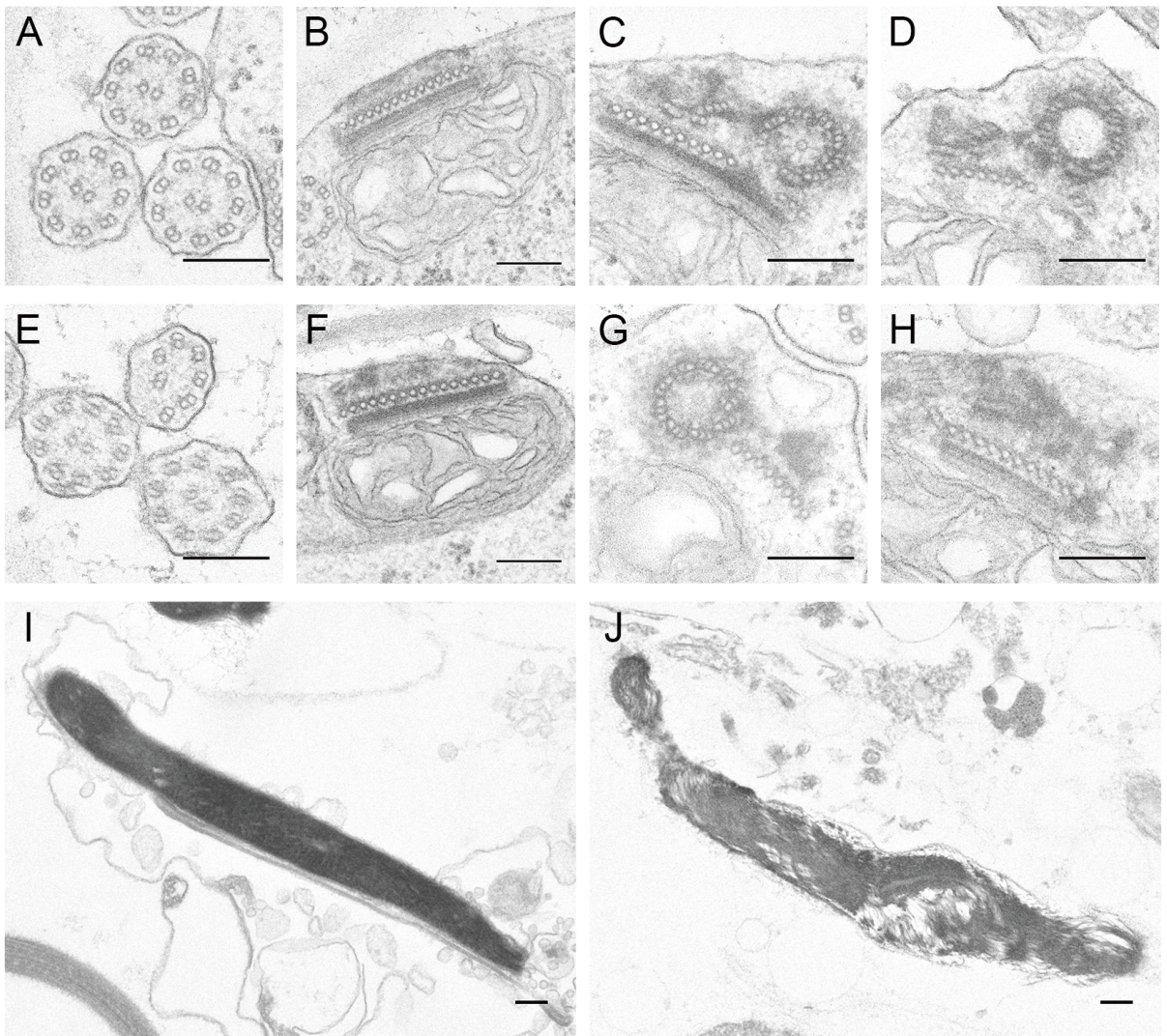


Fig. 2. Transmission electron microscopy (TEM) of spermatids and spermatozoa in wild type and *Mpbd10-1*.

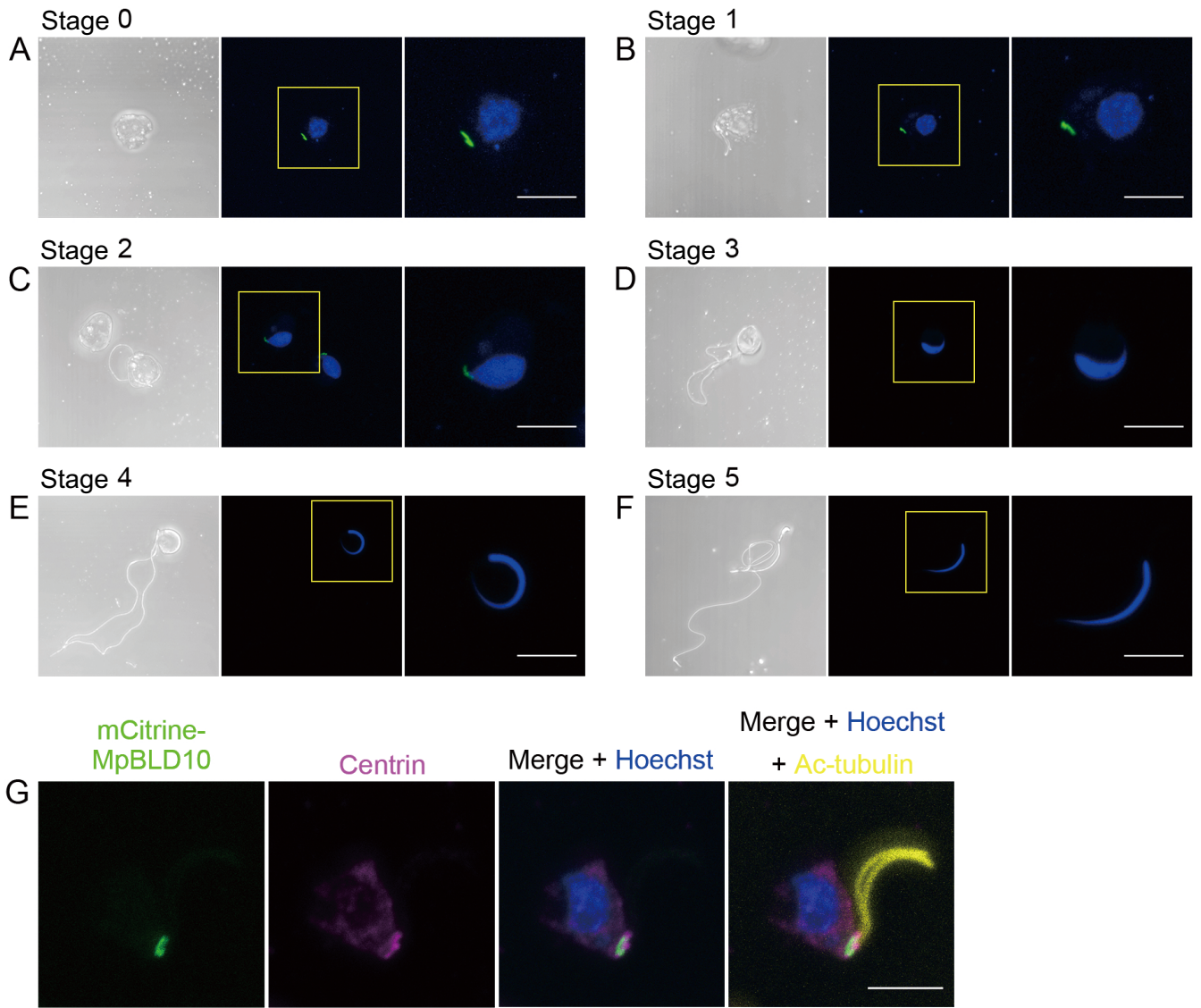


Fig 3. Subcellular localization of the MpBLD10 protein.

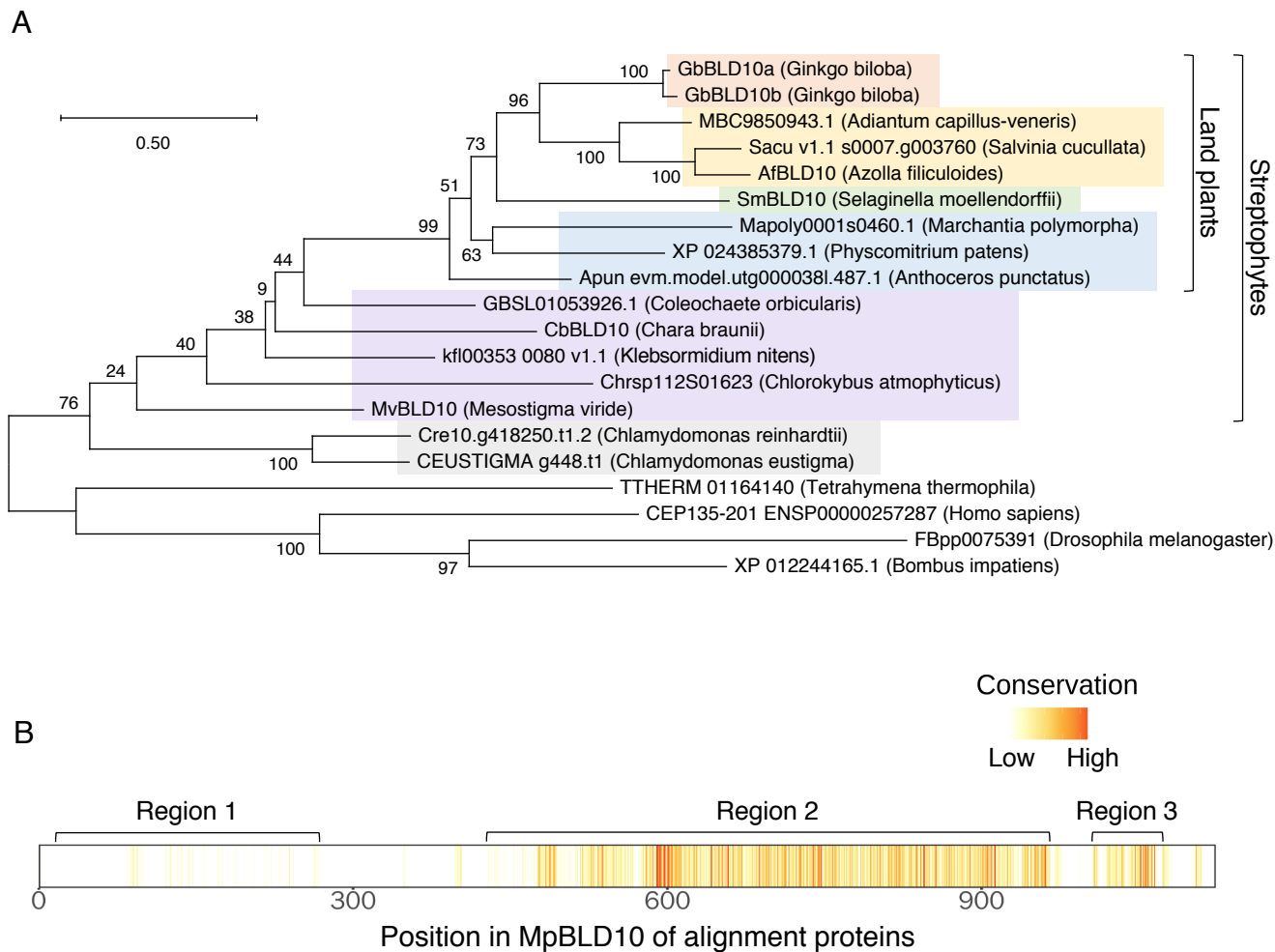


Fig. 4. Sequence comparisons of BLD10/CEP135 family proteins.

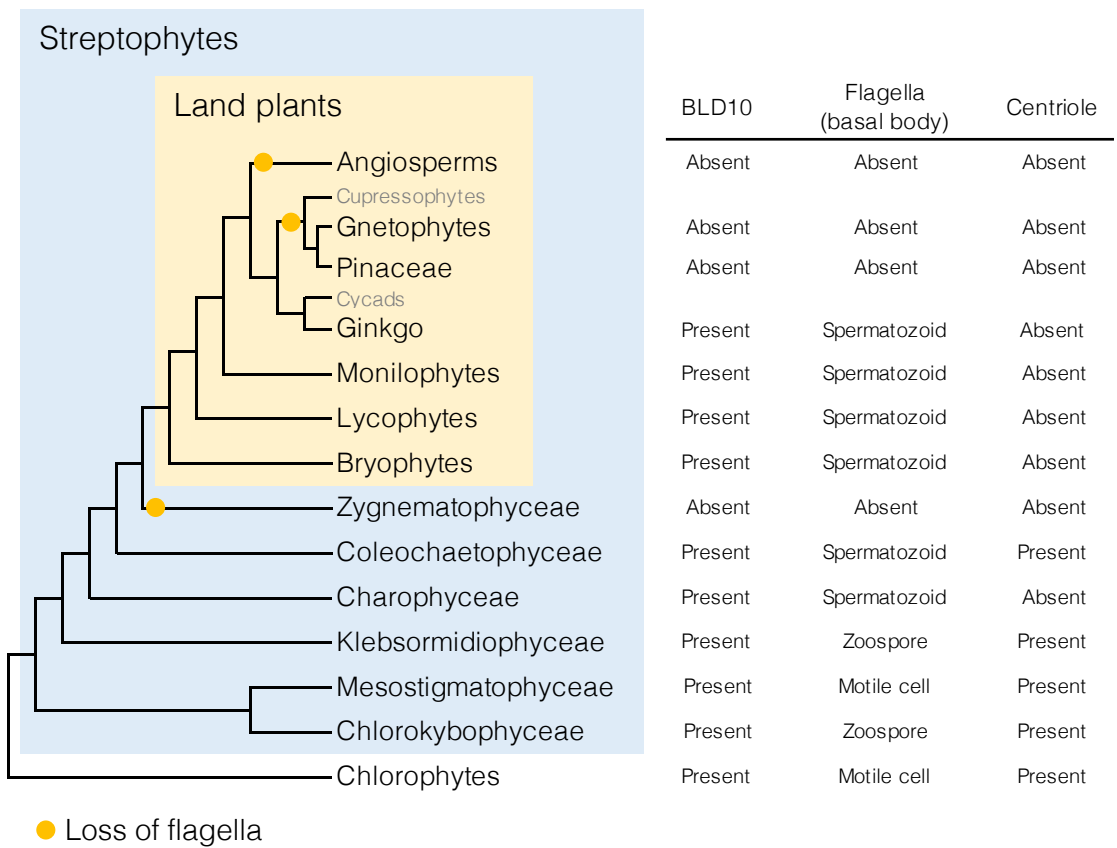


Fig. 5. Existence of BLD10 proteins, flagella, and basal body/centriole in the plant species.